Journal of Materials Chemistry A

PAPER

View Article Online
View Journal | View Issue

Published on 07 August 2014. Downloaded by Universiteit Utrecht on 27/10/2014 22:37:49.

Cite this: J. Mater. Chem. A, 2014, 2, 16285

Core–shell Co@C catalyzed MgH_2: enhanced dehydrogenation properties and its catalytic mechanism†

Ying Wang, Cuihua An, Yijing Wang,* Yanan Huang, Chengcheng Chen, Lifang Jiao and Huatang Yuan

Received 1st June 2014
Accepted 6th August 2014

DOI: 10.1039/c4ta02759k

www.rsc.org/MaterialsA

An efficient core–shell Co@C catalyst is synthesized through a solvothermal and subsequent annealing process. The as-synthesized Co@C consists of an 11 nm Co core and a 3 nm amorphous carbon shell. Nitrogen sorption isothermals show that Co@C has a surface area of 112.6 m^2 g^{-1} and a typical pore size of 4.8 nm. The catalytic effects of core–shell Co@C, which can significantly improve the dehydrogenation performance of MgH_2, are systematically investigated. With increasing amounts of Co@C (0, 3, 5, 10, 15 wt%), the dehydrogenation temperature of MgH_2 decreased. Its dehydrogenation kinetics are also improved, especially for the MgH_2–10%Co@C sample, which starts to release hydrogen at 168 °C. In fact, about 6.00 wt% hydrogen is released during its decomposition, and the activation energy of MgH_2–10%Co@C is determined to be 84.5 kJ mol^{-1}, 46.2% less than that of pure MgH_2. Mechanism analysis indicates that upon increasing the Co@C content, the decomposition of MgH_2 gradually occurs along lower-dimensional nucleation and growth. Moreover, the excellent thermal conductivity of the carbon shell in Co@C also contributes to the enhanced dehydrogenation performance of MgH_2.

Introduction

Hydrogen, the lightest element on the Earth, has a high energy efficiency of 142 MJ kg^{-1} and it is clean and renewable. Therefore, hydrogen is expected to play a vital role in future energy systems.[1,2] For practical usage, hydrogen storage media must be light, highly dense and affordable. MgH_2 has the potential to meet these requirements. Generally, the de/re-hydrogenation of MgH_2 is expressed as follows:

$$MgH_{2(s)} \underset{\text{rehydrogenation}}{\overset{\text{dehydrogenation}}{\rightleftharpoons}} Mg_{(s)} + H_{2(g)} \quad (1)$$

The theoretical hydrogen storage capacity of MgH_2 is 7.6 wt% (110 kg m^{-3}), large enough to satisfy the target of DOE. However, the commercial applications of MgH_2 still suffer from sluggish de/re-hydrogenation kinetics and high thermodynamic stability. The difficult thermal management of MgH_2 has also attracted much research attention.[3–5] Therefore, a proper method is needed to resolve these drawbacks and make MgH_2 more promising for both stationary and on-board energy storage. In practice, adding transition metals (TMs) is an effective strategy to modify the hydrogen storage properties of MgH_2.[6] For example, Hanada *et al.*[7] found that TM-catalyzed MgH_2 had better hydrogen desorption properties than pure MgH_2. A comparative study on the stability of MgH_2:Ti and MgH_2:Co was performed by Novakovic *et al.*,[8] which stated that the higher number of d-electrons in Co metal made it superior to Ti in destabilizing MgH_2. Other experiments also confirmed the favorable effects of Co on MgH_2. However, most of these studies were concerned only with bulk or irregular Co powders.[9–12]

It is well known that the same material can perform in obviously different ways, depending on its morphology and microstructure.[13–17] Generally, the core–shell structure shows improved physical and chemical properties compared to its bulk competitors.[18–21] The unique nature of the core–shell structure has led to numerous new applications in chemistry, bioscience and material science. In our previous work,[22] 1D nanorod structured Co@C, which was assembled with numerous core–shell particles, was successfully synthesized and used as a negative material for alkaline secondary batteries. Taking the unique structure of Co@C into consideration, it is expected to exhibit enhanced catalytic effects on the dehydrogenation properties of MgH_2.

In this work, we studied the catalytic effects of core–shell Co@C on the dehydrogenation performance of MgH_2. To gain

Institute of New Energy Material Chemistry, Collaborative Innovation Center of Chemical Science and Engineering (Tianjin), Key Laboratory of Advanced Energy Materials Chemistry (MOE), Nankai University, Tianjin 300071, P. R. China. E-mail: wangyj@nankai.edu.cn; Fax: +86 22 23503639; Tel: +86 22 23503639

† Electronic supplementary information (ESI) available: See DOI: 10.1039/c4ta02759k

Published on 07 August 2014. Downloaded by Universiteit Utrecht on 27/10/2014 22:37:49.

more insight in the effects of the doping amount, different weight ratios of Co@C (0, 3, 5, 10, 15 wt%) were added to MgH_2. The dehydrogenation performances of as-prepared MgH_2–Co@C composites were systematically investigated. Compared with pure MgH_2, the addition of Co@C remarkably enhanced the desorption properties of MgH_2, which can be explained from the standpoint of kinetics modification. The catalytic mechanism of Co@C is explored by using Johnson–Mehl–Avrami modeling, X-ray diffraction and X-ray photoelectron spectrometry.

Experimental

Synthesis of core–shell Co@C

$CoCl_2 \cdot 6H_2O$ and nitrilotriacetic acid (NTA) were commercially available from Alfa Aesar and used as received. Typically, $CoCl_2 \cdot 6H_2O$ (1.5 g) and NTA (0.6 g) were dissolved in 10 ml distilled water with continuous stirring. Then, 30 ml isopropyl alcohol was added and the mixture was stirred for another 10 min. The final solution was transferred into a Teflon-lined autoclave and heated at 180 °C for 6 h. The precipitation was collected by centrifugation, washed with water and ethanol repeatedly, and dried at 60 °C for 12 h under vacuum. This was followed by an annealing process at 500 °C for 2 h in an Ar atmosphere.

Synthesis of MgH_2–Co@C composites

Commercially available MgH_2 (Alfa Aesar) was pre-milled for 5 h under the protection of 0.5 MPa H_2 pressure. The ball to powder weight ratio was kept at 40 : 1 and ball-milled at 450 rpm. The MgH_2–Co@C composites were synthesized by mixing pre-milled MgH_2 with different weight ratios of Co@C (3, 5, 10, 15 wt%). Then, the mixtures were milled for another 2 h. For comparison, pure MgH_2 was milled under identical conditions without the addition of Co@C NPs.

Characterization

The structure and morphologies of as-prepared samples were characterized by X-ray diffraction (XRD, Rigaku D-Max-2500, Cu Kα radiation), Raman spectrometer (Renishaw inVia, excitation 514.5 nm), nitrogen adsorption and desorption isotherms (NOVA 2200e, Quantachrome), scanning electron microscopy (SEM JEOL JSM7500), transmission electron microscopy (TEM), scanning transmission electron microscopy (STEM), selected area electron diffraction (SAED), and high resolution transmission electron microscopy (HRTEM) on a JEOL JEM-2010FEF and X-ray photoelectron spectrometer (XPS, PHI 50000 Versaprobe, ULVAC PHI). The chemical composites of the as-prepared Co@C samples were determined by inductively coupled plasma optical emission spectrometry (ICP-OES, ICP-9000).

The dehydrogenation properties of MgH_2–Co@C composites were investigated by temperature-programmed desorption system (TPD, PX200) and differential scanning calorimetry (DSC, Q20P, TA). The isothermal desorption kinetics were performed on a home-made Sievert's instrument under an initial pressure of 0–0.05 MPa hydrogen.

Results and discussion

Structural and morphology characterization

The core–shell structure of as-synthesized Co@C was determined by TEM (Fig. 1a and b). Clearly, the Co@C NPs were self-assembled into a rod-like structure, which was about 100 nm in width. The SAED image (inset Fig. 1a) indicated that the as-synthesized Co@C had a polycrystalline nature. The rectangular region in Fig. 1a was selected for the HRTEM investigation. As shown in Fig. 1b, the lattice spaces of 2.05 Å and 1.76 Å, in the center, were assigned to the (111) and (200) planes of cubic Co metal. The d-space of 3.27 Å, in the edge, was consistent with the (002) plane of amorphous carbon. In other words, the central Co served as a core and the arrows in Fig. 1b point to the amorphous carbon shell. Clearly, the 3 nm amorphous carbon uniformly surrounded the surface of the 11 nm metallic Co core. The unique morphology of core–shell Co@C was further studied by SEM, which is shown in Fig. 1c and d. The irregular rod-like structure of Co@C (Fig. 1c) was consistent with the TEM results. Fig. 1d shows that the rod-like structure was further composed of numerous ultrafine Co@C NPs.

An XRD instrument was used to investigate the structure of as-synthesized Co@C NPs. As shown in Fig. 2a, the broad peak centered at 25° can be ascribed to the typical amorphous C (002) plane. The peaks at 44.1°, 51.7° and 76.0° can be ascribed to the (111), (200) and (220) planes of the cubic Co (JCPDS card no. 89-4307), respectively. The subdued diffraction peaks of Co were due to the coated carbon shell; thus, the core–shell structure of Co@C was further confirmed. The Co element content was obtained by ICP, and was 80.0% in the as-synthesized Co@C.

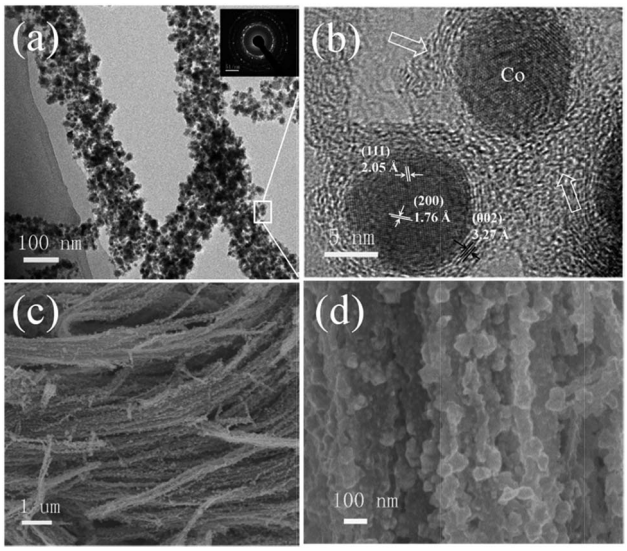

Fig. 1 (a) TEM, (b) HRTEM and (c and d) SEM images in different resolutions of the as-prepared Co@C sample. Inset (a) is the SAED pattern.

 This journal is © The Royal Society of Chemistry 2014

Published on 07 August 2014. Downloaded by Universiteit Utrecht on 27/10/2014 22:37:49.

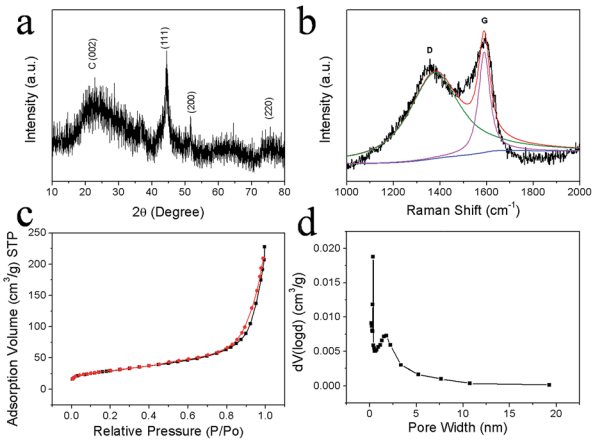

Fig. 2 (a) XRD, (b) Raman, (c) nitrogen sorption isothermals and (d) the corresponding pore width distribution pattern of the Co@C sample.

As an important approach to demonstrate the carbon state, the Raman spectrum is shown in Fig. 2b. Herein, Gaussian–Lorentzian fits were used to better illustrate the intensity, position and area of each bond. The peaks at 1355 cm^{-1} and 1589 cm^{-1} correspond to the D and G bands, respectively. Generally, the D band is activated by structural defects and disorders. Therefore, the D band is not observed in highly crystalline graphite. The G band is associated with E_{2g} phonons at the Brillouin zone and can be used to investigate graphitization. The intensity ratio of I_D/I_G in Co@C was 0.81, much higher than that of totally graphitized carbon.[23,24] Therefore, the as-synthesized carbon shell was in an amorphous state and contained numerous defects and disordered structure.

The specific surface area and pore size distribution of Co@C were determined by nitrogen sorption isothermals; the results are shown in Fig. 2c and d. The Brunauer–Emmett–Teller (BET) area of the synthesized Co@C was calculated to be 112.6 $m^2\ g^{-1}$. Generally, a large surface area can effectively prevent the aggregation of particles and provide a more intimate reaction between the catalyst and MgH_2. The pore size distribution showed a typical porous type and the mean pore size was 4.8 nm. Due to the porous structure of Co@C NPs, they can react with MgH_2 and hydrogen both on their surface and in the bulk of the materials.

XPS was used to investigate the surface electron escape of Co@C. It is clearly shown in Fig. 3a that the C 1s had a main peak at 284.78 eV, which was assigned to the carbon–carbon bonds. For the Co 2p curve (Fig. 3b) the peak at 778.18 eV was assigned to the metallic state of Co $2p_{3/2}$. The shoulder peak centered at 780.47 eV was caused by the surface oxidation of Co atoms.

Representative STEM pictures of the as-milled and dehydrogenated MgH_2–10%Co@C samples are illustrated in Fig. 4. Clearly, the rod-like structure of Co@C was broken during the ball-milling, but its core–shell structure was preserved and evenly distributed on the base of MgH_2/Mg during the sorption. After the dehydrogenation, both Co and C were well dispersed on the surface of elemental Mg. More importantly, the existence of well dispersed C can act as excellent heat exchanger during the sorption, which aids in the thermal management of MgH_2.

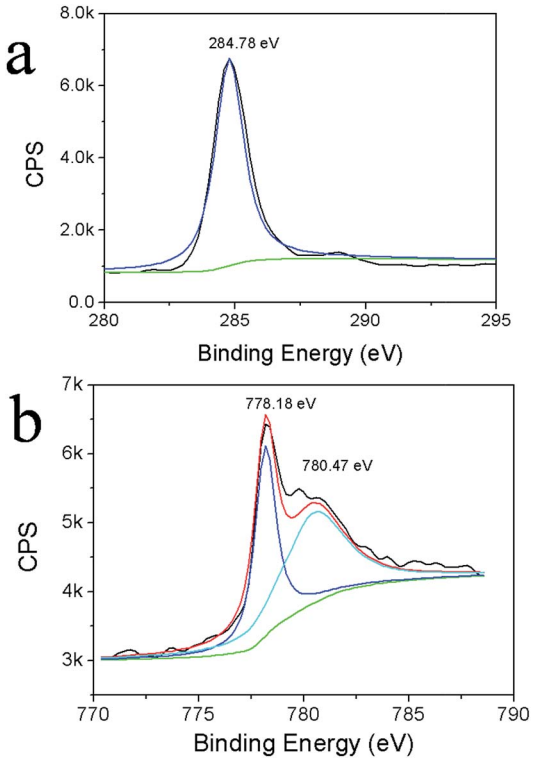

Fig. 3 (a) C 1s (b) Co 2p XPS traces of the Co@C NPS.

Dehydrogenation performance of MgH_2–Co@C composites

In order to study the enhanced effects of core–shell Co@C on the dehydrogenation performance of MgH_2, TPD investigations were carried out. Fig. 5a shows that the dehydrogenation of MgH_2 was a one-step process. The visible shoulder peaks were due to the bimodal particle phenomenon.[23] Pure MgH_2 started to release hydrogen at about 301 °C, which is a very high temperature for practical applications. However, the onset dehydrogenation temperature of MgH_2 significantly decreased with the addition of core–shell Co@C. Even the 3 wt% Co@C doped MgH_2 sample began to release hydrogen at a much lower temperature of 200 °C, about 101 °C lower than that of pure MgH_2. This downward trend was more obvious with the increasing amount of Co@C. Detailed information about the operating temperatures is listed in Table 1. The significantly decreased operating temperature of MgH_2 indicated that core–shell Co@C NPs can clearly improve the desorption properties of MgH_2, with performance superior to that of nano-Co,[7] carbon,[24,25] and MWCNT/Co.[26]

The quantitative dehydrogenation capacities of the of MgH_2–Co@C compositions were calculated and are shown in Fig. 5b. With increasing amounts of Co@C, MgH_2 was able to desorb hydrogen at lower temperatures; however, unfortunately, the dehydrogenation capacity of MgH_2 also gradually decreased. As shown in Table 1, upon heating to 500 °C about 6.84 wt% hydrogen was released from pure MgH_2. This value decreased to 6.25 wt% for MgH_2–3%Co@C, 6.20 wt% for MgH_2–5%Co@C, 6.00 wt% for MgH_2–10%Co@C, and finally to 5.78 wt% for the

Published on 07 August 2014. Downloaded by Universiteit Utrecht on 27/10/2014 22:37:49.

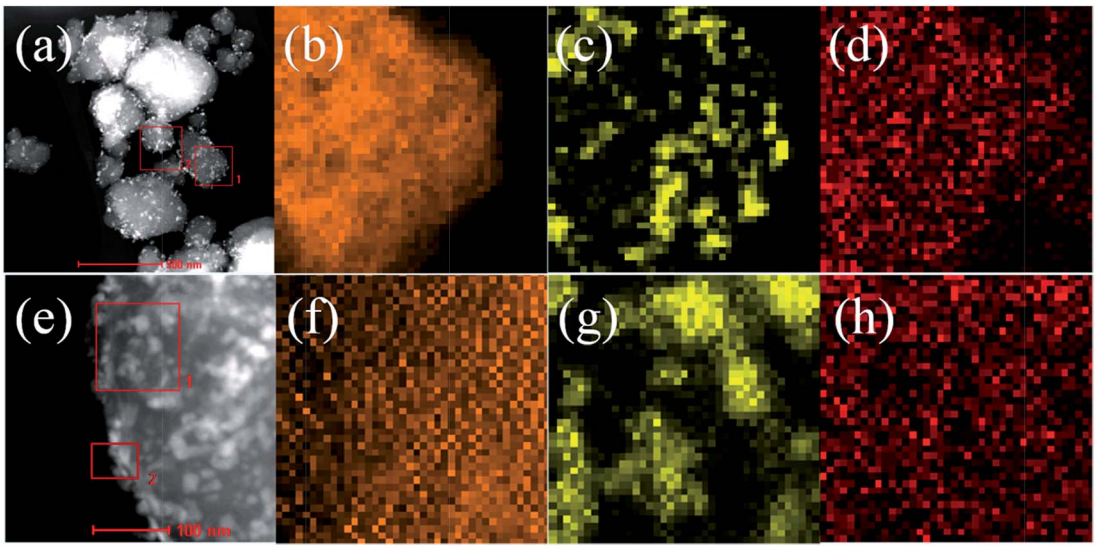

Fig. 4 Representative STEM images of the MgH_2–10%Co@C samples (a–d) as-milled, (e and f) after dehydrogenation. Mg, Co and C elements mapping are in brown, yellow and red, respectively.

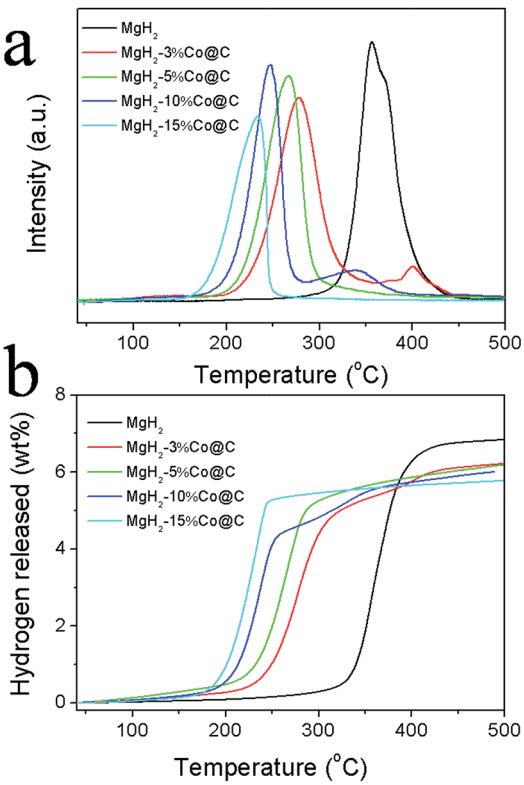

Fig. 5 (a) Thermal desorption curves and (b) the corresponding hydrogen desorption patterns of as-prepared pure MgH_2 and 3 wt%, 5 wt%, 10 wt%, and 15 wt% Co@C doped MgH_2 samples. Heating at 2 °C min^{-1} under Ar atmosphere.

MgH_2–15%Co@C sample. The decreased capacity was attributed to the high amount of additives.

Isothermal desorption experiments can clearly illustrate dehydrogenation kinetics; therefore, the isothermal desorption patterns were analysed and are presented in Fig. 6. Fig. 6a shows that core–shell Co@C had positive effects in accelerating the dehydrogenation kinetics of MgH_2. Upon increasing the additive amount of Co@C, the desorption rate of MgH_2 also increased. Notably, the MgH_2–15%Co@C sample released about 5.42 wt% hydrogen within 10 min. When heated for 25 min, the MgH_2–10%Co@C sample liberated the highest hydrogen value of 5.8 wt%. At the same time, about 5.51, 5.23 and 4.12 wt% hydrogen were released from MgH_2–15%Co@C, MgH_2–5%Co@C and MgH_2–3%Co@C, respectively. No visible hydrogen was released from pure MgH_2. The total desorption capacity showed a modest shift to a lower value with increasing weight ratio of Co@C composites, from 6.24 wt% for MgH_2–3% Co@C to 5.78 wt% for the MgH_2–15%Co@C sample. This trend agreed with the TPD results; however, the pure MgH_2 only released about 3.8 wt% hydrogen during the test, due to its high operating temperature.

Table 1 Onset dehydrogenation temperature and the released capacity of hydrogen for as-milled samples

Sample name	Onset temperature (°C)	H_2 capacity (wt%)
MgH_2	301	6.84
MgH_2–3%Co@C	200	6.25
MgH_2–5%Co@C	185	6.20
MgH_2–10%Co@C	168	6.00
MgH_2–15%Co@C	143	5.78

The Johnson–Mehl–Avrami (JMA) equation is widely used to study the nucleation mechanism of solid-state reactions.[27] Generally, the JMA equation is expressed as follows:

$$\ln[-\ln(1 - \alpha(t))] = n \ln(t) + n \ln(k) \quad (2)$$

 This journal is © The Royal Society of Chemistry 2014

Published on 07 August 2014. Downloaded by Universiteit Utrecht on 27/10/2014 22:37:49.

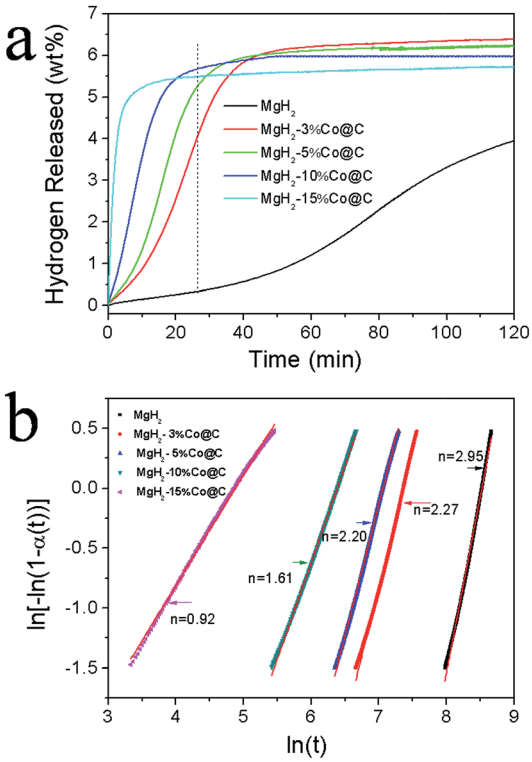

Fig. 6 (a) Isothermal dehydrogenation curves of the pure MgH_2, MgH_2–3%Co@C, MgH_2–5%Co@C, MgH_2–10%Co@C and MgH_2–15% Co@C composites at 300 °C and (b) their JMA fitting plots.

here t is the reaction time, $\alpha(t)$ is the dehydrogenated fraction at time t, k is the phase transformation constant, and n is the Avrami exponent that relates to the dimensionality of the MgH_2/Mg transformational mechanism. Clearly, when $\alpha(t)$ varies from 0.2 to 0.8 the $\ln[-\ln(1-\alpha(t))]$ shows a straight line against $\ln(t)$. Therefore, the JMA equation was well suited to investigate the desorption mechanism of pure MgH_2 and MgH_2–Co@C composites. Interestingly, the Avrami exponent n was shifted from 2.95 for pure MgH_2 to 2.27 and 2.20 for the MgH_2–3% Co@C and MgH_2–5%Co@C composites, continuously to 1.61 for the MgH_2–10%Co@C sample, and finally to 0.92 for the MgH_2–15%Co@C sample. It is well known that different values of n illustrate different types of nucleation and growth mechanism. For pure MgH_2, n was close to 3 (2.95); therefore, the dehydrogenation of MgH_2 had a three-dimensional growth with increased nucleation rate.[28] After the addition of 3 and 5 wt% Co@C, n was close to 2 (2.27 or 2.20), indicating that the dehydrogenation had a two-dimensional nucleation and growth mechanism.[29] For the MgH_2–10%Co@C sample n was 1.61, close to 1.5; therefore, it had a three dimensional growth with zero nucleation growth.[30] As the doping content of Co@C increased to 15 wt%, n decreased to about 1 (0.92) which indicates nucleation and growth along one-dimensional dislocation lines.[31,32] Generally, hydrogen diffuses more easily along lower-dimensional defects. The different nucleation and growth types of MgH_2–Co@C composites can explain the enhanced desorption kinetics of Co@C doped MgH_2 samples.

Catalytic mechanism

It is well known that an amorphous carbon shell not only contributes to enhanced heat conductivity but also buffers the volume change of Co and maintains its core–shell structure during sorption. Moreover, the existence of irregular defects in the carbon shell provides more channels and active sites for hydrogen diffusion. At the same time, the central Co has an almost full d-band electron structure. The spin-splitting of the Co-d electron results in a narrower E_g than in pure MgH_2 and leads to high structural stability of the compound.[8] The unique electronic structure of Co can form a Co–H transition-state intermediate with hydrogen, which is stronger than the Mg–H bond and further leads to a destabilization effect on MgH_2. Herein, the detailed catalytic mechanism of Co@C on MgH_2 is also proposed.

Taking both the operating temperature and the desorption capacity into consideration, the representative MgH_2–10% Co@C sample was selected to further study the catalytic mechanism of core–shell Co@C. The XRD patterns of pure MgH_2 and MgH_2–10%Co@C are shown in Fig. 7. All the as-milled samples showed a main phase of MgH_2 (JCPDS card no. 12-697), indicating that MgH_2 was well maintained during the ball-milling. For the MgH_2–10%Co@C sample the diffraction peak at 44.1° was assigned to the (111) plane of Co@C; therefore, Co@C remained intact during the synthesis procedure. Moreover, the diffraction peaks of MgH_2–10%Co@C were broader and weaker. Table 2 shows that the lattice parameters of as-milled pure MgH_2 were $a = b = 4.52$ Å and $c = 3.02$ Å, which agreed with the standard values for tetragonal MgH_2. For the MgH_2–10%Co@C sample the lattice parameters slightly decreased to lower values of $a = b = 4.51$ Å and $c = 3.01$ Å. This demonstrated that Co@C may cause more metal associated defects in the MgH_2 structure, which plays a crucial role in atomic transport. The grain size was 11.6 nm for pure MgH_2 and 8.70 nm for the MgH_2–10%Co@C sample, determined by the Scherrer equation. The smaller size of the MgH_2–10%Co@C sample can partially explain the subdued MgH_2 peaks in the XRD curves. It is known that the reaction kinetics are enhanced with decreasing particle size, due to the

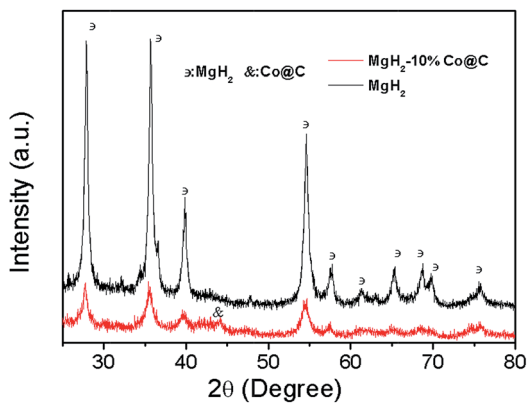

Fig. 7 XRD images of the as-milled pure MgH_2 and MgH_2–10%Co@C samples.

Published on 07 August 2014. Downloaded by Universiteit Utrecht on 27/10/2014 22:37:49.

Table 2 Representative cell parameters and grain sizes of the as-milled pure MgH_2 and MgH_2–10%Co@C samples

Sample name	Lattice parameters (Å) $a = b$	c	Grain size (nm)
MgH_2	4.52	3.02	11.6
MgH_2–10%Co@C	4.51	3.01	8.70

larger surface to volume ratio and shorter solid-state diffusion distance for hydrogen.

Significant improvements in the hydrogen storage properties of MgH_2 may be caused by thermodynamic or/and kinetic modifications. Here, kinetic modifications seemed to be more feasible in the particle size distribution (11.6–8.7 nm). As an important kinetic factor, apparent activation energy (E_a) can vividly illustrate the energy barrier for the dehydrogenation of MgH_2. Therefore, the Kissinger equation is used to determine the E_a, which is expressed as follows:

$$d\left[\ln\left(\frac{\beta}{T_m^2}\right)\right]\Big/d\left(\frac{1}{T_m}\right) = \frac{-E_a}{R} \quad (3)$$

where β is the heating rate, T_m is the peak temperature and E_a is the apparent activation energy. The non-isothermal DSC curves were used to determine the E_a of pure MgH_2 and MgH_2–10%Co@C samples. The typical DSC curves of pure MgH_2 and MgH_2–10%Co@C are shown in Fig. S1.† When heated at 5 °C min^{-1}, the peak temperature of MgH_2–10%Co@C was 316.1 °C, about 43.2 °C lower than that of pure MgH_2. The obviously decreased peak temperature further confirmed the superior catalytic effects of Co@C. The data used to calculate the E_a of samples is listed in Table S1.† Fig. 8 showed that E_a for the MgH_2–10%Co@C composites was 84.5 kJ mol^{-1}, which was more favorable than that of pure MgH_2 (157.1 kJ mol^{-1}) and other previously reported values.[7,33–35] The obviously decreased E_a implies that the enhanced kinetics of the MgH_2–10%Co@C sample are caused by the decreased energy barrier during the desorption reaction.

Fig. 9 shows the XPS spectra of as-synthesized and dehydrogenated pure MgH_2 and MgH_2–10%Co@C composites. The magnified Mg 2p curves of as-milled samples are shown in Fig. 9a. Clearly, both the pure MgH_2 and MgH_2–10%Co@C show a strong peak centered at 50.12 eV, which corresponds to the binding energy of MgH_2.[36] The XPS spectra of dehydrogenated Mg 2p are displayed in Fig. 9b. The binding energy of the MgH_2–10%Co@C sample was 49.5 eV, assigned to the metallic Mg. For pure MgH_2 the binding energy of Mg 2p was slightly higher, a visible shoulder peak appeared at 51.1 eV which indicated a mixture of divalent Mg.[37,38] Therefore, the decomposition of pure MgH_2 was incomplete. After dehydrogenation, the Co 2p peak of the MgH_2–10% Co@C sample was located at 778.7 eV, indicating the existence of metallic Co. Moreover, the C 1s peak, at 284.8 eV, was consistent with the as-synthesized Co@C sample. Therefore, Co@C remained intact during the dehydrogenation.

The dehydrogenated samples were further collected for XRD measurement. Fig. S2† shows that the main peaks for the pure MgH_2 and MgH_2–10%Co@C samples were distributed to the phase of metallic Mg. However, for pure MgH_2 there was still some visible MgH_2, which can explain its lower dehydrogenation capacity. For the MgH_2–10%Co@C sample, the diffraction peak at 44.1° was due to the existence of Co@C.

Fig. S3† shows the SEM images of the pure MgH_2 and MgH_2–Co@C samples. The as-milled pure MgH_2 experienced serious agglomeration, and most of the larger particles were comprised of smaller particles (ranging in size from several to hundreds of nanometers). The MgH_2 particle sizes grew further during the dehydrogenation. On the other hand, the MgH_2–10%Co@C particles were well distributed. Therefore, Co@C can effectively prevent aggregation and particle growth of the MgH_2–10%Co@C sample during dehydrogenation.

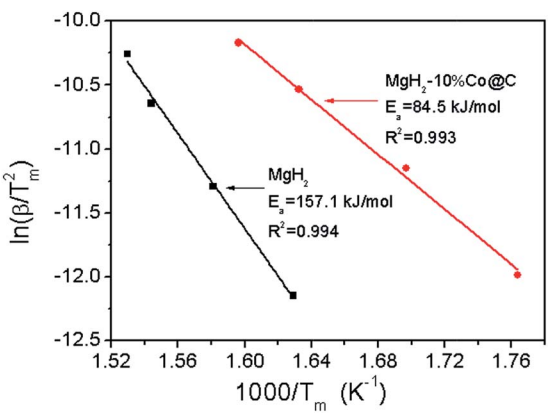

Fig. 8 E_a of the as-prepared pure MgH_2 and MgH_2–10%Co@C composites, obtained by Kissinger method at heating rates of 2, 5, 10, 15 °C min^{-1}.

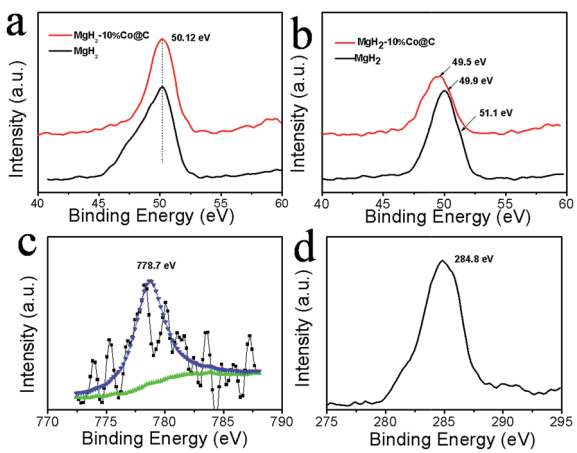

Fig. 9 XPS spectra of (a) as-milled and (b) dehydrogenated Mg 2p peaks. (c) Co 2p and (d) C 1s patterns of the dehydrogenated MgH_2–10%Co@C sample.

 This journal is © The Royal Society of Chemistry 2014

Published on 07 August 2014. Downloaded by Universiteit Utrecht on 27/10/2014 22:37:49.

Conclusions

In summary, core–shell Co@C NPs were synthesized *via* a facile hydrothermal method. Morphology characterization indicated that the as-synthesized Co@C was about 14 nm in diameter, and was composed of an 11 nm Co core and a 3 nm carbon shell. The as-synthesized Co@C showed enhanced catalytic effects on the dehydrogenation performance of MgH_2. The onset dehydrogenation temperature of MgH_2 significantly decreased with increasing amounts of Co@C catalyst, *i.e.* from 301 °C for pure MgH_2 to the lowest value of 148 °C for the MgH_2–15%Co@C sample. Moreover, the Co@C can improve the dehydrogenation kinetics of MgH_2. Further studies showed that the enhanced dehydrogenation properties of MgH_2–Co@C composites were due to the obviously decreased E_as, which were 84.5 and 157.1 kJ mol^{-1} for MgH_2–10%Co@C and pure MgH_2. Theoretical modeling of the experimental data indicated that the dehydrogenation of MgH_2 proceeded through lower-dimensional growth after the addition of core–shell Co@C.

Acknowledgements

This work gratefully acknowledges the financial support received from MOST projects (2010CB631303, 2012AA051901), NSFC (5117108), 111 Project (B12015) and MOE ((IRT-13R30)).

Notes and references

1 M. Dresselhaus and I. Thomas, *Nature*, 2001, **414**, 332–337.
2 L. Schlapbach and A. Züttel, *Nature*, 2001, **414**, 353–358.
3 A. F. Dalebrook, W. Gan, M. Grasemann, S. Moret and G. Laurenczy, *Chem. Commun.*, 2013, **49**, 8735–8751.
4 R. Bardhan, A. M. Ruminski, A. Brand and J. J. Urban, *Energy Environ. Sci.*, 2011, **4**, 4882.
5 Y. S. Au, M. K. Obbink, S. Srinivasan, P. C. M. M. Magusin, K. P. de Jong and P. E. de Jongh, *Adv. Funct. Mater.*, 2014, **24**, 3604–3611.
6 J. Cui, H. Wang, J. Liu, L. Ouyang, Q. Zhang, D. Sun, X. Yao and M. Zhu, *J. Mater. Chem. A*, 2013, **1**, 5603–5611.
7 N. Hanada, T. Ichikawa and H. Fujii, *J. Phys. Chem. B*, 2005, **109**, 7188–7194.
8 N. Novakovic, J. G. Novakovic, L. Matovic, M. Manasijevic, I. Radisavljevic, B. P. Mamula and N. Ivanovic, *Int. J. Hydrogen Energy*, 2010, **35**, 598–608.
9 J. Cui, J. Liu, H. Wang, L. Ouyang, D. Sun, m. zhu and X. Yao, *J. Mater. Chem. A*, 2014, **2**, 9645–9655.
10 M. G. Verón, H. Troiani and F. C. Gennari, *Carbon*, 2011, **49**, 2413–2423.
11 J. Mao, Z. Guo, X. Yu, H. Liu, Z. Wu and J. Ni, *Int. J. Hydrogen Energy*, 2010, **35**, 4569–4575.
12 M. G. Verón, A. M. Condó and F. C. Gennari, *Int. J. Hydrogen Energy*, 2013, **38**, 973–981.
13 C. Zhu and T. Akiyama, *Cryst. Growth Des.*, 2012, **12**, 4043–4052.
14 X. Wang, J. Zhuang, Q. Peng and Y. Li, *Nature*, 2005, **437**, 121–124.
15 C. An, G. Liu, L. Li, Y. Wang, C. Chen, Y. Wang, L.-F. Jiao and H. Yuan, *Nanoscale*, 2014, **6**, 3223–3230.
16 M. L. Christian and K. F. Aguey-Zinsou, *ACS Nano*, 2012, **6**, 7739–7751.
17 H. Liu and G. Wang, *J. Mater. Chem. A*, 2014, **2**, 9955–9959.
18 F. Qiu, L. Li, G. Liu, C. Xu, C. An, Y. Xu, Y. Wang, Y. Huang, C. Chen, L. Jiao and H. Yuan, *Chem.–Asian. J.*, 2014, **9**, 487–493.
19 F. Qiu, Y. Dai, L. Li, C. Xu, Y. Huang, C. Chen, Y. Wang, L. Jiao and H. Yuan, *Int. J. Hydrogen Energy*, 2014, **39**, 436–441.
20 F. Qiu, G. Liu, L. Li, Y. Wang, C. Xu, C. An, C. Chen, Y. Xu, Y. Huang, Y. Wang, L. Jiao and H. Yuan, *Chem.–Eur. J.*, 2014, **20**, 505–509.
21 X. Wu, H. Niu, S. Fu, J. Song, C. Mao, S. Zhang, D. Zhang and C. Chen, *J. Mater. Chem. A*, 2014, **2**, 6790–6795.
22 C. An, Y. Wang, Y. Xu, Y. Wang, Y. Huang, L. Jiao and H. Yuan, *ACS App. Mater. Interfaces*, 2014, **6**, 3863–3869.
23 C. X. Shang and Z. X. Guo, *J. Power Sources*, 2004, **129**, 73–80.
24 C. Z. Wu, P. Wang, X. Yao, C. Liu, D. M. Chen, G. Q. Lu and H. M. Cheng, *J. Alloys Compd.*, 2006, **420**, 278–282.
25 C. Z. Wu, P. Wang, X. Yao, C. Liu, D. M. Chen, G. Q. Lu and H. M. Cheng, *J. Alloys Compd.*, 2006, **414**, 259–264.
26 M. G. Veron, H. Troiani and F. C. Gennari, *Carbon*, 2011, **49**, 2413–2423.
27 J. W. Christian, *The Theory of Transformations in Metals and Alloys*, Pergamon, New York, 2nd edn, 1975.
28 K. L. Sahoo, A. K. Panda, S. Das and V. Rao, *Mater. Lett.*, 2004, **58**, 316–320.
29 G. Barkhordarian, T. Klassen and R. Bormann, *J. Alloys Compd.*, 2006, **407**, 249–255.
30 C. Wu, P. Wang, X. Yao, C. Liu, D. Chen, G. Q. Lu and H. Cheng, *J. Phys. Chem. B*, 2005, **109**, 22217–22221.
31 K.-J. Jeon, H. R. Moon, A. M. Ruminski, B. Jiang, C. Kisielowski, R. Bardhan and J. J. Urban, *Nature mater.*, 2011, **10**, 286–290.
32 Y. Liu, Y. Pang, X. Zhang, Y. Zhou, M. Gao and H. Pan, *Int. J. Hydrogen Energy*, 2012, **37**, 18148–18154.
33 Y. Jia, S. Han, W. Zhang, X. Zhao, P. Sun, Y. Liu, H. Shi and J. Wang, *Int. J. Hydrogen Energy*, 2013, **38**, 2352–2356.
34 H. Liu, X. Wang, Y. Liu, Z. Dong, G. Cao, S. Li and M. Yan, *J. Mater. Chem. A*, 2013, **1**, 12527–12535.
35 Z. Zhao-Karger, J. Hu, A. Roth, D. Wang, C. Kubel, W. Lohstroh and M. Fichtner, *Chem. Commun.*, 2010, **46**, 8353–8355.
36 S. Gupta, I. Z. Hlova, T. Kobayashi, R. V. Denys, F. Chen, I. Y. Zavaliy, M. Pruski and V. K. Pecharsky, *Chem. Commun.*, 2013, **49**, 828–830.
37 K. S. Jung, D. H. Kim, E. Y. Lee and K. S. Lee, *Catal. Today*, 2007, **120**, 270–275.
38 O. Friedrichs, L. Kolodziejczyk, J. C. Sánchez-López, C. López-Cartés and A. Fernández, *J. Alloys Compd.*, 2007, **434–435**, 721–724.